Journal of Thermal Analysis and Calorimetry (2022) 147:11373–11389
https://doi.org/10.1007/s10973-022-11352-1

Thermal performance of a circular tube embedded with TBVG inserts: an experimental study

Rahul Bahuguna[1] · K. K. S. Mer[2] · Manoj Kumar[3] · Sunil Chamoli[2]

Received: 5 April 2021 / Accepted: 30 March 2022 / Published online: 9 May 2022

Abstract

The results of various geometrical and flow parameters on thermal energy transfer and performance of tube heat exchangers with solid and perforated "triple-blade vortex generator" insert are presented in this study. Pitch ratio = 1,2,3,4, blade angle = 45°, and perforation index = 0%, 25% are the parameters used in the experiment. The experiments are carried out over a wide range of Reynolds numbers, ranging from 6000 to 24,000. A three-dimensional numerical analysis is also performed to gain a better understanding of fluid flow behavior and heat transfer mechanisms. The results show that using the triple-blade vortex generator insert improves the performance of a heat exchanger. The heat transfer escalation detected in comparison with a simple heat exchanger with a plain tube is in the range of 2.4–4.35, maximum for pitch ratio of 1 and 0% perforation index and a minimum for pitch ratio of 4 and 25% perforation index. The friction factor varies from 0.43 to 3.15, lowest for pitch ratio of 4 and a 25% perforation index and the highest for pitch ratio of 1 and 0% perforation index. The maximum thermal performance of 1.16 is achieved with a pitch ratio of 1 and a perforation index of 25%. For the prediction of Nusselt number, friction factor, and the thermal performance factor of the tubular heat exchanger with triple-blade vortex generator inserts, statistical correlations are developed using experimental data.

Keywords Heat transfer · Friction factor · Thermal performance factor · Triple-blade vortex generator · Perforation

List of symbols

A_c	Cross-sectional area of tube, m^2
A_o	Cross-sectional area of orifice, m^2
A_s	Surface area of tube, m^2
C_d	Coefficient of discharge for orifice meter
C_p	Specific heat of air at constant pressure, J kg^{-1} K^{-1}
D	Internal diameter of the tube m
d_h	Diameter of hole for perforation, m
h	Convective heat transfer coefficient, W m^{-2} K^{-1}
k	Thermal conductivity of air, W m^{-1} K^{-1}
L	Length of the tube, m
$\dot{m}$	Mass flow rate of fluid, kg s^{-1}
ΔP	Pressure drop across test section, Pa
ΔP_o	Pressure drop across the orifice plate, Pa
P_a	Atmospheric pressure, Pa
Q	Heat transfer rate, W
T_a	Ambient temperature, K
T_i	Fluid inlet temperature, K
T_o	Fluid outlet temperature, K
ΔT_m	Log mean temperature difference, K
T_{wm}	Mean wall temperature, K
T_w	Local wall temperature, K
V	Velocity of air, m/s
σ	Stefan–Boltzmann constant, W m^{-2} K^{-4}
ρ	Density of air, kg m^{-3}
μ	Dynamic viscosity, kg m^{-s}
β	Ratio of orifice diameter to tube internal diameter
f	Friction factor
f_s	Friction factor of smooth tube
Re	Reynolds number
l	Spacing between two consecutive insert geometry, m
Pr	Prandtl number
Nu	Nusselt number
Nu_s	Nusselt number of smooth tube
T_w	Local wall temperature, °C

✉ Rahul Bahuguna
rahul.bahuguna25@gmail.com

[1] Department of Thermal Engineering, Faculty of Technology, Veer Madho Singh Bhandari Uttarakhand Technical University, Dehradun, Uttarakhand, India 248007

[2] Department of Mechanical Engineering, GBPIET, Pauri Garhwal, Uttarakhand, India 246194

[3] Department of Mechanical Engineering, DIT University, Dehradun, Uttarakhand, India 248009

T_b	Bulk mean temperature, °C
T_{wm}	Wall mean temperature, °C
t	Thickness of insert blade, m
TR	Thickness ratio
PR	Pitch ratio
PI	Perforation index, %
BA	Blade angle, °
TPF	Thermal performance factor
TBVG	Triple-blade vortex generator

Introduction

The use of heat exchangers is widespread in industrial and domestic equipments. Optimizing heat transfer enhancement techniques and in turn making the heat exchangers more efficient can be beneficial at an enormous magnitude. Therefore, increasing the thermal performance of heat exchangers has been a topic of research attracting numerous researchers for the last few decades.

In a conventional heat exchanger unit installed in the chemical industry as shown in Fig. 1, significant energy in the form of heat is under-utilized and released to the surroundings due to the lower thermal performance of the heat exchanger. To increase the thermal performance of the heat exchanger, many researchers have proposed different methods, primarily passive techniques for a broad spectrum of Reynolds number (Re), and have achieved substantial results. Improving heat transfer using physical disturbances has been a prevailing area of study and experimentation for the research community active in this field. Several insert geometries using various configurations and parameters have proved their distinct effect on the outcome of heat transfer, friction factor (f) or pressure drop, and thermal performance factor (TPF) of the heat exchanger. El-Sayed et al. [1] used

Fig. 1 A Typical shell and tube heat exchanger used in a chemical industry

longitudinal interrupted fins as turbulence promotors with inline, continuous, and staggered arrangements. According to the findings, a maximum pressure drop occurs with a staggered design, resulting in lower thermal performance. Among different insert geometries, twisted tapes are one of the most commonly used geometries reported by several researchers. Works reported by Bas et al. [2], Bhuiya et al. [3], and Bhuiya et al. [4] used twisted tapes as inserts with different combinations of twist ratio and width ratio. Their investigations reported the effect of multiple twisted tapes on heat transfer, f, and TPF and revealed that heat transfer increased with a decrease in twist ratio.

Although incorporating twisted tapes yields significant results, there is still room for performance improvement. Moreover, twisted tapes primarily affect the core fluid region inside the tube, and the tube–wall region is widely intact; hence, various modifications have been made in twisted tape geometries. Researchers like Promvonge [6] and Promvonge et al. [7] studied the effects of twisted tape with conical insert and twisted tape with uniform coiled wire insert, respectively. They reported a notable improvement in heat transfer in respect of a simple heat exchanger having a plain tube. Eiamsa-ard et al. [5] examined the effects of a compound insert by using twisted tape with rings. This geometry influences the core and wall fluid stream, which hinders the development of the thermal boundary layer. The study revealed a significant improvement in thermal performance over a plain tube heat exchanger. Eiamsa-ard et al. [8] and Bhuiya et al. [9] incorporated serrated twisted tapes and twisted tapes with perforations, respectively, in their experimental investigation. According to the study, incorporating perforation into the geometries significantly reduces pressure drop, thereby improving thermohydraulic performance. Furthermore, the f in the perforated and serrated twisted tape was lower than the standard twisted tape. In a study, Pal and Saha [10] revealed that ribbed tubes with twisted tapes having oblique teeth yield significantly higher heat transfer improvements than individual enhancement techniques. Zhang et al. [11] employed self-rotating twisted tapes as inserts, indicating that the self-rotating inserts improved heat transfer and had anti-scaling and descaling properties. It is also noted that twisted tapes perform better in laminar than turbulent regions. Salem et al. [12] used a helical twisted tape insert in a double pipe heat exchanger and reported that increasing the height ratio and decreasing the pitch ratio (PR) of a helical twisted tape inserts increased the Nusselt number (Nu) and friction; the maximum hydro-thermal performance index was obtained at a height ratio of 0.667. The performance of peripheral u-cut twisted tapes with and without ring inserts was examined by Abolarin et al. [13]. It is reported that in the transitional flow regime, increasing the depth cut ratio and decreasing the spacing ratio of the rings considerably increased the heat transfer rate. Chu

et al. [14] examined the impact of various shapes of cuts in twisted tape. The enhancements in *Nu* and *f* brought about by u-cut were identical to those brought out by isosceles V-cut configurations, according to experimental results. Fagr et al. [15] investigated the effect of a conventional twisted tape with various decreasing tapered twisted tapes. It was reported that inserting standard twisted tape and reducing tapered twisted tapes resulted in a negligible improvement in thermal performance. The thermal performance of a tube fitted with twisted tape inserts with dimples and perforations was investigated experimentally by Dagdevir and Ozceyhan [16]. The results of the experiment revealed that the novel dimpled twisted tape insert outperforms previous twisted tape geometries in terms of heat transfer performance. Chang al. [17] investigated the performance of a square duct with inclined slots and ribs paired with twist tape. The average increase in *Nu* was found to be 3.8–4.2 times that of a smooth tube, at the expense of an increase in frictional losses of 32.5–40.2 times that of a smooth tube. Singh et al. [18] studied the double-pipe heat exchanger with dimpled twisted tape as inserts and found the highest increase in heat transfer of 1.82 times that of a plain tube heat exchanger, with a dimple diameter to depth ratio of 0.005 m providing the best thermal performance.

Investigators also looked into a few novel geometries to further increase the thermal performance of the heat exchanger. Promvonge & Eiamsa-ard [19] used conical turbulators and found that closely spaced turbulator produces better outcomes concerning heat transfer than widely spaced turbulators. Kongkaitpaiboon et al. [20] employed a perforated conical ring as an insert geometry and reported that it performed better than a smooth tube heat exchanger. Gunes et al. [21] used triangular cross-sectioned coiled wire in their study with a scope confined to surface alteration resulting in less significant findings. The circular rings were employed as insert geometry by Kongkaitpaiboon et al. [22], who varied the geometrical parameters *PR* and diameter ratio. It was reported that the lowest value of *PR* and diameter ratio pertains to maximum heat transfer. In their investigation, Eiamsa-ard and Promvonge [23] used double-sided delta wing tape and found that employing the double-sided delta wings increased the *Nu* and *f* by 165% percent and 14.8 times, respectively, over the plain tube, with a maximum TPF of 1.19. Kumar et al. [24] used a solid and perforated circular disk as insert geometry and found that using perforation in the circular disk geometry reduces *f*, resulting in improved thermal performance. Singh et al. [25] examined perforated hollow circular cylinder inserts and found that the heat transfer rate is 150–230% higher than that of plain tube values; the TPF is in the range of 1.21–1.47, maximum at diameter ratio of 0.65, and a perforation index (*PI*) of 8%. Straight tape with solid and perforated curved winglets was utilized as inserts by Skullong et al. [26]. They reported that perforated curved winglet tapes had a 9% higher thermal enhancement factor than solid curved winglet tapes. Wijayanta et al. [27] used double-sided delta-wing tape as inserts and found that at a higher wing width ratio, the double-sided tape inserts had higher convective heat transfer enhancements and frictional losses than the longitudinal strip insert and plane tube; the maximum thermohydraulic performance factor was 1.15 at wing width ratio of 0.63. Chamoli et al. [28] used anchor-shaped inserts in their numerical study, which resulted in a significant increase in heat transfer and f, with a maximum thermal enhancement factor of 1.72. Gururatana and Skullong [29] employed airfoil-shaped inserts, claiming that heat transfer increase by utilizing a 45° inclination angle insert is three times better than a conventional tube heat exchanger. Nakhchi et al. [30] used perforated louvered strips as inserts and found that *Nu* for double perforated louvered strip inserts is higher than for single perforated louvered strip inserts for the same slant angles; the double perforated louvered strip insert has the highest thermal enhancement factor of 1.84. Liang et al. [31] used a center tapered wavy tape insert and reported that a maximum performance enhancement criterion of 2.62 is achieved in respect of a plain tube heat exchanger. Hong et al. [32] examined the transverse corrugated tube (TCT) using twin and triple wire coils in an experimental setting. The *Nu* enhancement ratio for TCT and TCT combined with multiple wire coil inserts ranged from 1.35 to 1.49 and 1.74 to 2.61, respectively, while the maximum performance evaluation criterion was found to be 1.09 when utilizing twin wire coils. Paneliya et al. [33] employed X-shaped inserts and found that compared to a simple twisted tape, X-shaped inserts demonstrated a 1.27-fold increase in heat transfer. Multiple helical tape inserts were employed by Bahuguna et al. [34] and an increase in thermal performance of 1.23 times than the smooth tube heat exchanger was reported for twist ratio 2 and number of tapes 1. Singh et al. [35] employed conical ring turbulators with protrusion and dimple roughness and found that for protrusion roughness of 0.006 m diameter and pitch space of 0.240 m, the best thermohydraulic factor of 2.44 was reached. Zarei et al. [36] investigated the heat transfer increase produced by a Koflo inline mixture as a swirl creator placed in a circular tube with a crossing angle of 90° and 120° between the blades. It was reported that raising the crossing angle reduces heat transfer enhancement. Ebrahimi and Naranjani [37] numerically studied the flat-plate channel configured with pyramidal protrusions in laminar range and reported that the overall efficiency of the channels with pyramidal protrusions is improved by 12.0–169.4% compared to the plain channel for the conditions studied here. Ebrahimi and Roohi [38] investigated numerically the flow patterns inside mini twisted oval tubes (TOTs) heated by constant-temperature walls and recorded that the improvement in synergy between

velocity and temperature gradient and lower irreversibility cause heat transfer enhancement for TOTs. Manoram et al. [39] numerically investigated the influence of dimples and its various parameters on the thermal efficiency of the solar collector and reported a 2.5 times improvement in *Nu* and 11.1% increase in *f* concerning smooth tube. Bhattacharyya et al. [40] studied the effect of broken twisted tape on thermal performance of triangular axial corrugated tubes and reported that for all examined cases the performance factors are larger than one.

From the vast discussion of the literature review, it is noticed that the vortex generators are capable of providing disturbances in the core as well as in the wall region of the fluid flow inside the tube and have performed better. The circular rings, flapped wings, and wiglets significantly improve the performance of different insert geometries embedded heat exchangers over the smooth tube. In light of these findings, the vortex generator inserts appear to be a promising alternative to other inserts. Hence, it is critical to develop a new vortex-inducing insert geometry that is capable of increasing heat transfer by disrupting the thermal boundary layer in the heated wall region, allowing the heat exchanger's thermal performance to improve. To propose a novel vortex-inducing insert geometry, a modification in the solid disk is provided by making it into three equal blades and keeping these blades at a certain angle for providing better fluid flow streamlining over them. Furthermore, the perforation in the blades is done for reducing the pressure drop across the tube, thereby increasing the TPF of the heat exchanger. This novel insert geometry used in the present research work is named as "triple-blade vortex generator" (TBVG). This paper investigates and presents the effect of various geometrical and flow parameters of TBVG inserts on heat transfer, fluid flow, and thermal performance of tubular heat exchangers.

Experimental facility

Insert geometry

The TBVG insert is used as a turbulence promoter inside the heat exchanger tube in this work. Different geometrical and flow parameters of TBVG inserts embedded heat exchanger tube used in the experiments are stated in Table 1. Pictorial views of the TBVG insert are shown in Fig. 2, and its dimensional details are presented in Fig. 3.

Experimental setup

Experimental apparatus primarily composed of an inlet section, also known as a calming section, a test section with TBVG inserts, a heating arrangement for the test section, and a blower for supplying air. The length of the inlet section is 2.5 m, which ensures that a fully developed fluid flow enters the test section. The test section which is 1.5 m long comes after the inlet section. A heating mechanism is used in the test section, after which insulation is applied to the tube's outer surface. A total of sixteen T-type thermocouples are used to measure temperatures using a data logger which is linked to a computer having LabVIEW software. Twelve thermocouples are fixed near the wall of the tube to measure the tube wall temperature: one at the inlet and three at the exit of flow to determine the inlet and outlet temperature of the air. Thermocouples on the tube's wall are fixed at the fluid–wall interface. The thermocouple is fixed in a hole bored in the tube wall up to the closest point of interaction between the fluid and the tube wall. The pressure drop across the test section is measured with a digital micromanometer connected to knobs at the inlet and exit of the test segment. The flow system follows the test segment, which includes a 3-HP blower with a 3-phase power supply. Before the blower, a flow measuring device is connected, which comprises an orifice plate and a u-tube manometer using distilled water as the manometric fluid. A flow control valve is installed near the blower to regulate the rate of fluid flow during experimentation. Figure 4 shows a schematic diagram of the experimental test setup.

Table 1 Experimental parameters used in the present study

S. no.	Parameter	Specification	Range
1	Pitch ratio (*PR*)	l/D	1, 2, 3 and 4
2	Blade angle (*BA*)	Angle	45°
3	Thickness ratio (*TR*)	t/D	0.0075
4	Perforation index (*PI*)	P_A/T_A	0% and 25%
5	Reynolds number (*Re*)	Flow parameter	6000–24,000

The approach proposed by Kline and McClintock [41] is used to calculate the uncertainty in the measurements of different parameters during experiments. The calculated uncertainty for different parameters, i.e., *Re*, *Nu,* and *f,* is ± 7.42%, ± 2.87%, and ± 7.45%, respectively. The uncertainty analysis is presented in "Appendix".

Data reduction and validation

The air is used as a working fluid in the experiments, which is forced to flow in the heated test segment. The data points are recorded when the system reaches a quasi-steady state. When there is no change in any of the measurement quantities recorded within 5 min, the steady state is assumed to have been reached. The heat losses from the tube to the surroundings are neglected; thus, in a steady

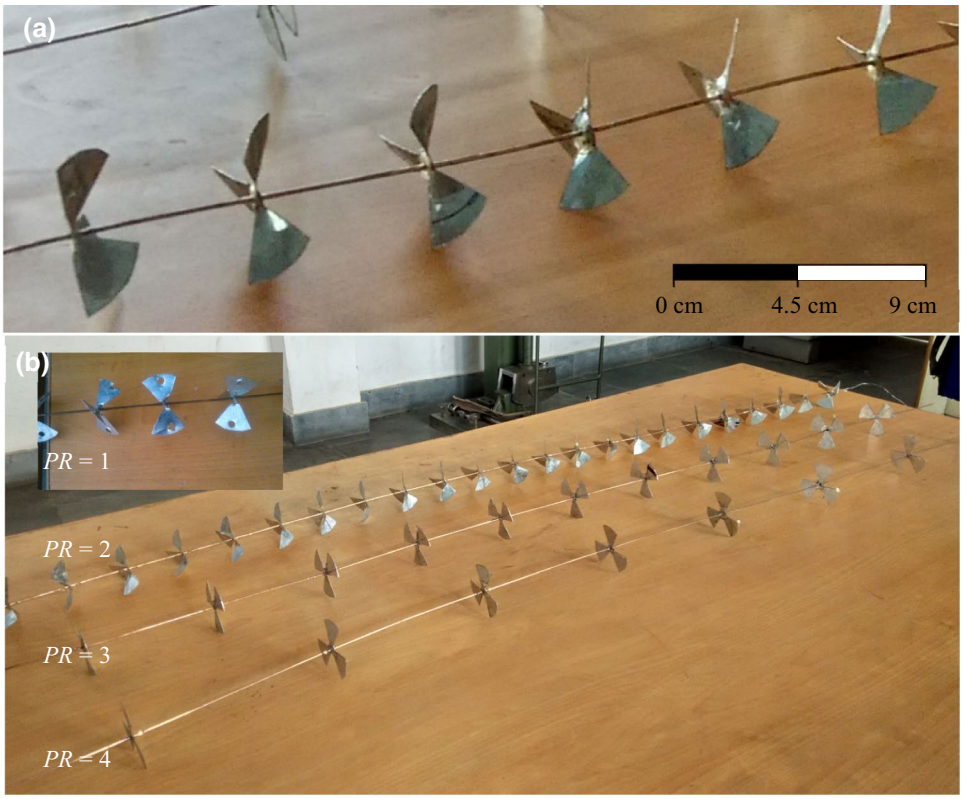

Fig. 2 **a.** Pictorial view of TBVG insert. **b.** Pictorial view of TBVG insert with different *PR*

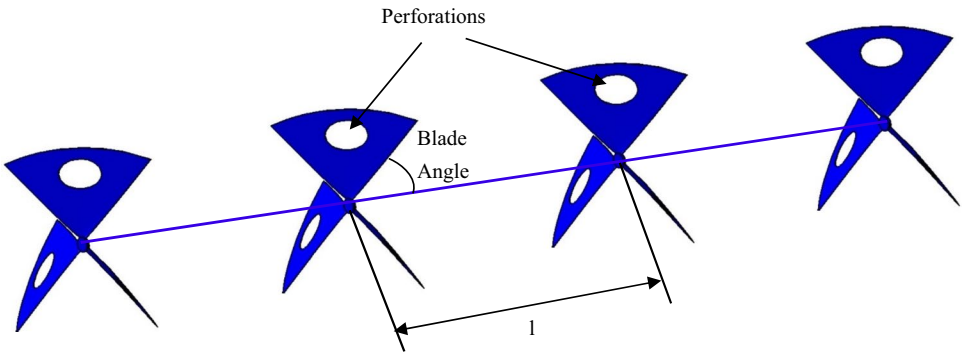

Fig. 3 Dimensional details of TBVG insert

state the convective heat transfer is equal to the heat carried away by the flowing air and is expressed as:

$$Q_{\text{air}} = Q_{\text{conv}} \tag{1}$$

where

$$Q_{\text{air}} = \dot{m} C_{\text{p}} \left(T_{\text{o}} - T_{\text{i}} \right) \tag{2}$$

where T_{i} and T_{o} are the temperatures of air at the inlet and outlet of the test segment. T_{o} is calculated by area-weighted averaging of the temperatures gauged by the thermocouples, three in number, positioned in the airstream at the outlet of the test section, and is given as:

$$T_{\text{o}} = \frac{A_{\text{c1}} T_{\text{o1}} + A_{\text{c2}} T_{\text{o2}} + A_{\text{c3}} T_{\text{o3}}}{A_{\text{c}}} \tag{3}$$

where T_{o1}, T_{o2}, and T_{o3} are the temperatures gauged at the outlet of transverse section area realm A_{c1}, A_{c2}, and A_{c3}, respectively, and A_{c} is the transverse section area of the tube.

The convection heat transfer rate from the test segment or heat exchanger tube wall is given by:

$$Q_{\text{conv}} = h A_{\text{s}} \Delta T_{\text{m}} \tag{4}$$

where ΔT_{m} is log mean temperature difference of heat exchanger tube and is given as:

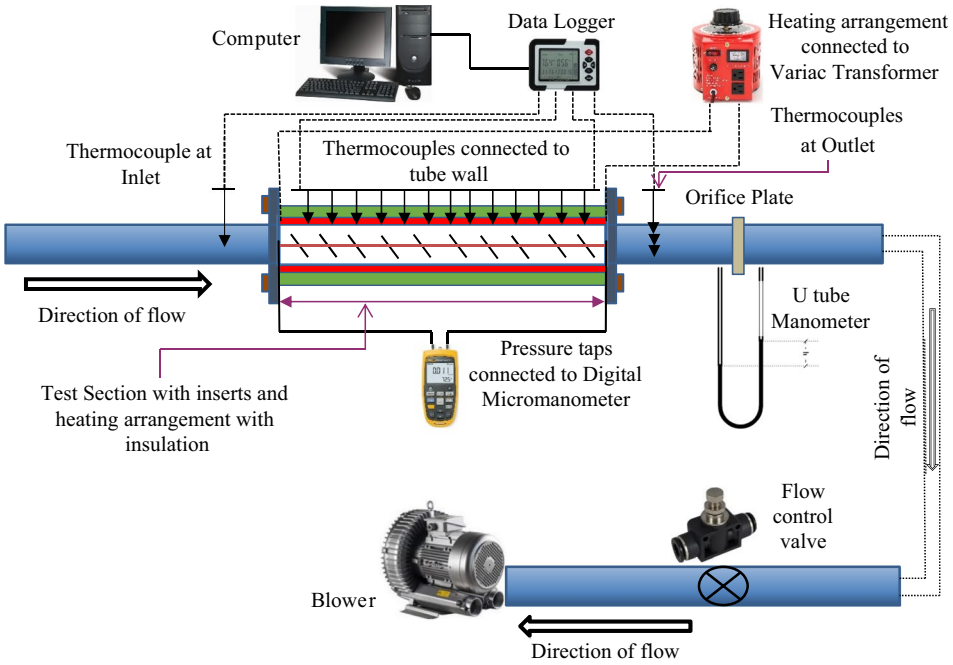

Fig. 4 Schematic view of the experimental setup

$$\Delta T_{\mathrm{m}} = \frac{\Delta T_{\mathrm{i}} - \Delta T_{\mathrm{o}}}{\left(\ln\left(\frac{\Delta T_i}{\Delta T_o}\right)\right)} \tag{5}$$

where ΔT_{i} and ΔT_{o} are the differences in temperatures of the mean wall temperature of the tube (T_{wm}) with T_{i} and $T_{\mathrm{o,}}$ respectively.T_{wm} is calculated by averaging the temperature readings of all the thermocouples (total 12) placed on the wall surface of the test segment and is given as:

$$T_{\mathrm{wm}} = \frac{\sum T_{\mathrm{w}}}{12} \tag{6}$$

The average heat transfer coefficient (h) is calculated as:

$$h = \frac{\dot{m} C_{\mathrm{p}} \left(T_{\mathrm{o}} - T_{\mathrm{i}}\right)}{A_{\mathrm{s}} \Delta T_{\mathrm{m}}} \tag{7}$$

where $\dot{m}$, the mass flow rate of air, is calculated as:

$$\dot{m} = C_{\mathrm{d}} A_{\mathrm{o}} \left[\frac{2\rho \Delta P_{\mathrm{o}}}{1 - \beta^4}\right]^{0.5} \tag{8}$$

Mean fluid velocity (V) inside the tube is determined as:

$$V = \frac{\dot{m}}{\rho A_{\mathrm{c}}} \tag{9}$$

The values of Re at different fluid flow rate are obtained by the following standard equation:

$$\mathrm{Re} = \frac{\rho \mathrm{V D}}{\mu} \tag{10}$$

The average Nu is further calculated as:

$$\mathrm{Nu} = \frac{h \mathrm{D}}{k} \tag{11}$$

The values of f is obtained as:

$$f = \frac{\Delta P}{\left[\left(\frac{\mathrm{L}}{\mathrm{D}}\right)\left(\frac{\rho \mathrm{V}^2}{2}\right)\right]} \tag{12}$$

TPF of the tubular heat exchanger is then calculated as:

$$\mathrm{TPF} = \frac{\mathrm{Nu}/\mathrm{Nu}_s}{(f/f_{\mathrm{s}})^{1/3}} \tag{13}$$

All thermophysical properties of air are taken at fluid bulk mean temperature. Smooth tube validation is performed before collecting heat transfer and f data of TBVG inserts embedded tube. The validation of the smooth tube assures the correctness of the methodology and the instruments used in the experimental work. The average values of Nu and f are determined for smooth tube and are compared with the predicted values from the smooth tube correlations available in the literature and depicted in Eqs. 14 and 15 for f and Nu, respectively.

Blasius equation

$$f_s = 0.316\mathrm{Re}^{-0.25} \quad (14)$$

Dittus–Boelter equation

$$\mathrm{Nu}_s = 0.023\mathrm{Re}^{0.8}\mathrm{Pr}^{0.4} \quad (15)$$

The variation of ± 5% and ± 9% from the predicted values is obtained for the *Nu* and *f,* respectively, and is shown in Fig. 5. This confirms the accuracy of data measurement and validates the test facility.

Numerical simulation

A numerical simulation is done to better understand the fluid flow behavior and heat transfer mechanism inside the heat exchanger tube with TBVG inserts. For numerical simulation, the geometric parameters of the TBVG insert are kept the same as in experimental work. At constant $Re = 6000$, TBVG inserts with $PR = 1$ and $PI = 25\%$ are used to achieve the fluid flow pattern. During the numerical simulation, the following assumptions are taken into account.

- The flow is 3D, steady and incompressible.
- No variation in pressure along the y-direction.
- No shear force along the y-direction.
- The body's gravitational force has been ignored.
- It is a fully developed flow at the test section's inlet.
- The fluid's axial heat conduction is negligible.
- At atmospheric pressure and temperature, the thermophysical properties of air do not change.

Turbulent flows are characterized by fluctuating velocity fields. There can be small-scale and high-frequency changes in the transported quantities. Variations in velocity fields cause momentum and energy to be mixed; hence, these quantities vary as well. To remove small scales, the governing equations can be modified that are computationally little expensive to resolve. The k-ε models include independent transport equations for the turbulence length scale, or some comparable parameter, as well as the turbulent kinetic energy, in which turbulent production and dissipation balance. Therefore, a typical (RNG) k-ε model is chosen for simulations because several studies [8, 19, 20, 22, 30] have used the (RNG) k-ε model to produce nearly accurate results in their numerical simulations. The RANS (Reynolds averaged Navier–Stokes) equations and energy equations are applied for simulation. These governing equations along with k and ε are solved using Ansys Fluent, which is a CFD software based on the finite volume method. In the Cartesian tensor system, these governing equations can be written as:

Continuity equation:

$$\frac{\partial}{\partial x_i}(\rho u_i) = 0$$

Momentum equation:

$$\frac{\partial}{\partial x_i}\left(\rho u_j u_j\right) = -\frac{\partial p}{\partial x_i} + \frac{\partial}{\partial x_j}\left[\mu\left(\frac{\partial u_i}{\partial x_j} + \frac{\partial u_j}{\partial x_i}\right)\right] + \frac{\partial}{\partial x_j}\left(-\rho\overline{u_i' u_j'}\right)$$

Energy equation:

$$\frac{\partial}{\partial x_i}\left(\rho u_j T\right) = \frac{\partial}{\partial x_j}\left(\left(\Gamma + \Gamma_t\right)\frac{\partial T}{\partial x_j}\right)$$

where $\Gamma + \Gamma_t$ are the molecular thermal diffusivity and turbulent thermal diffusivity respectively and are given by,

$$\Gamma = \mu/Pr \quad \Gamma_t = \mu_t/Pr_t$$

Transport equations used for Renormalization group (RNG) *k*-ε model, to determine turbulence kinetic energy, *k* and rate of dissipation, ε for computational domain analysis, are:

$$\frac{\partial}{\partial x_i}\left(\rho k u_i\right) = \frac{\partial}{\partial x_j}\left(\alpha_k \mu_{\mathrm{eff}}\frac{\partial k}{\partial x_j}\right) + G_k - \rho\varepsilon$$

and

$$\frac{\partial}{\partial x_i}\left(\rho\varepsilon u_i\right) = \frac{\partial}{\partial x_j}\left(\alpha_k \mu_{\mathrm{eff}}\frac{\partial \varepsilon}{\partial x_j}\right) + C_{1\varepsilon}\frac{\varepsilon}{k}(G_k) - C_{2\varepsilon}\rho\frac{\varepsilon^2}{k} - R_\varepsilon$$

where G_k represents the generation of turbulence kinetic energy due to mean velocity gradients and is expressed as

$$G_k = -\rho\overline{u_i' u_j'}\frac{\partial u_j}{\partial x_i}$$

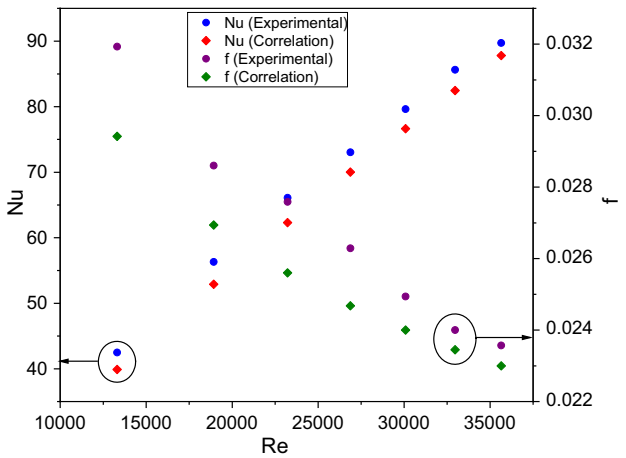

Fig. 5 Validation of smooth tube for *Nu* and *f*

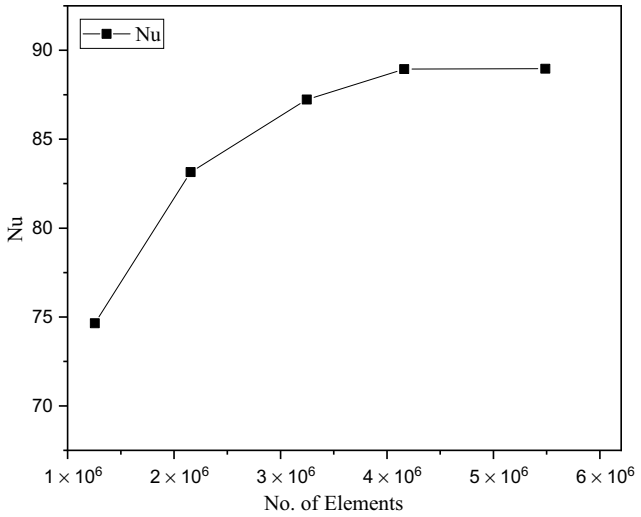

Fig. 6 Results of grid independence test in graphical form

μ_{eff} represents the effective turbulent viscosity and is given as:

$$\mu_{\text{eff}} = \mu + \mu_{\text{t}}$$

The turbulent viscosity, μ_{t}, is computed by combining k and ε as follows:

$$\mu_{\text{t}} = \rho C_{\mu} \frac{k^2}{\varepsilon}$$

where $C_{\mu} = 0.09$ is constant. The quantities α_k and α_{ε} are the inverse effective turbulent Prandtl numbers for k and ε, respectively. The model constants have the following values, $C_{1\varepsilon} = 1.44$, $C_{2\varepsilon} = 1.92$, $\alpha_{\text{k}} = 1$ and $\alpha_{\varepsilon} = 1.30$. An elaborate explanation of these standard governing equations is provided in [42].

A SIMPLE algorithm is used to link the pressure and velocity. QUICK, which is a higher-order differencing scheme, is used to discretize governing equations. For all variables, the convergence criteria for normalized residual values are set to less than 10^{-7}. The grid independence test is conducted using the solution refinement method. As shown in Fig. 6, the variance in *Nu* is negligible after 4.16×10^6 cells; hence, mesh with 4.16×10^6 cell numbers will be analyzed for simulation.

The part section of meshed modeled geometry of TBVG inserts is shown in Fig. 7. The boundary conditions applied to a numerical model for simulation are given in Table 2.

Table 2 Boundary conditions for a geometric model

S. no.	Name	Boundary conditions
1	Inlet	Velocity inlet, and temperature of air of 300 K
2	Outlet	Outflow
3	Outer surface	Insulated
4	Inner surface	No slip wall, and uniform constant heat flux of 1000 W m^{-2}

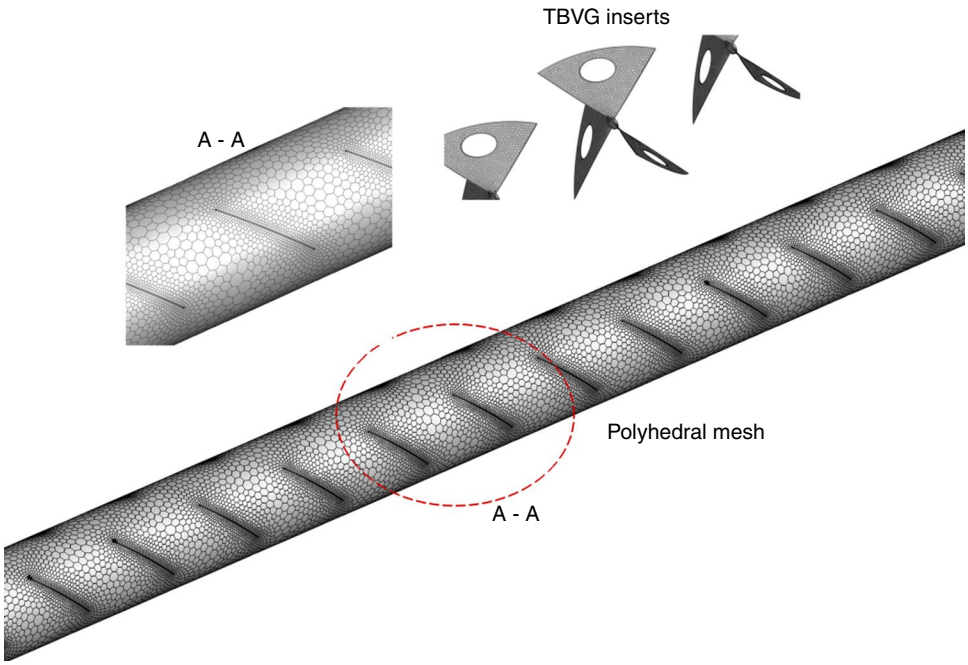

Fig. 7 Mesh generation of TBVG inserts geometry

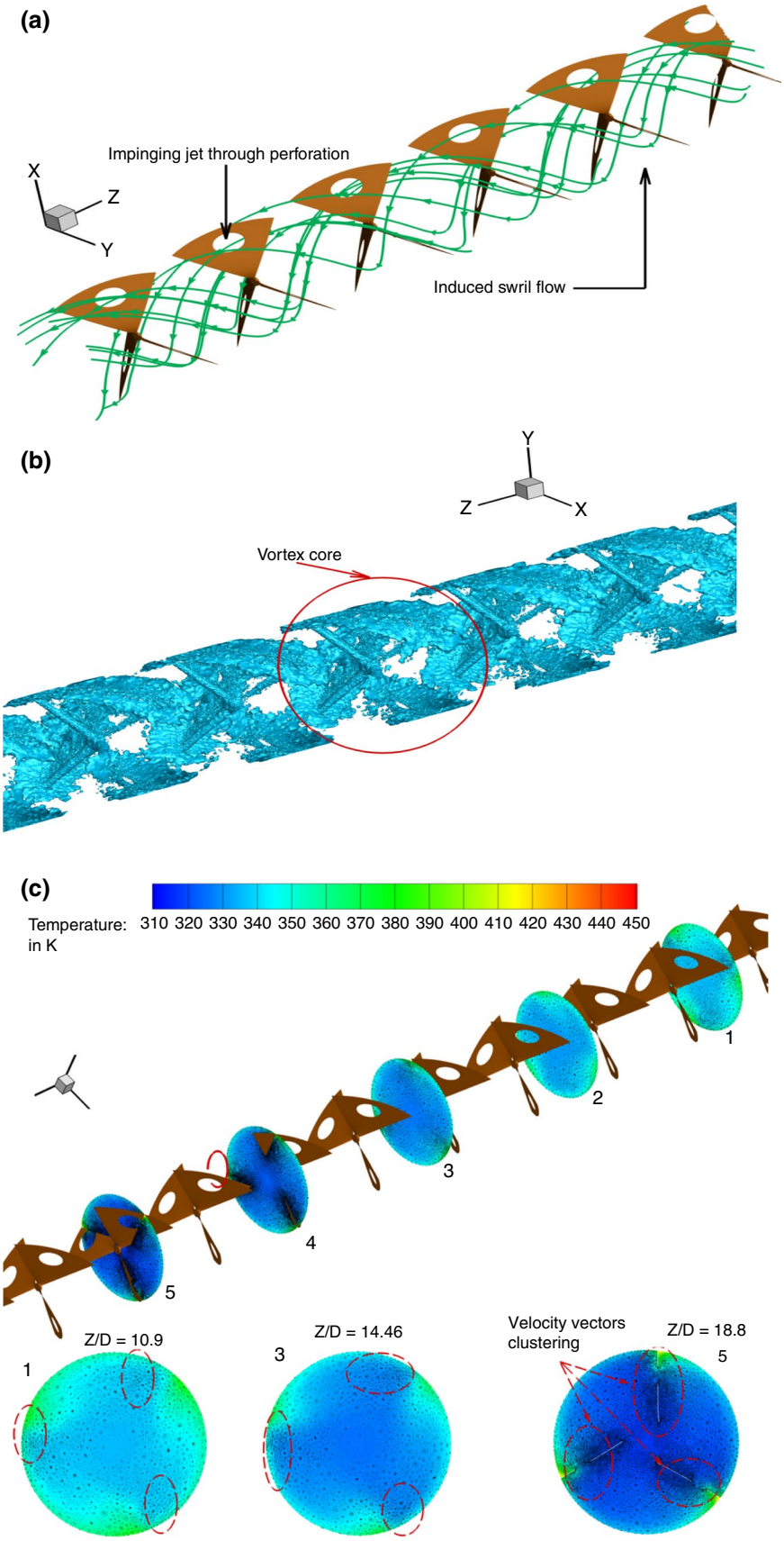

Fig. 8 **a.** 3D streamlines, **b.** Vortex core regions, **c.** Temperature contours along with velocity vectors, for TBVG insert integrated tube with $PR = 1$ and $PI = 25\%$, at $Re = 6000$

Numerical results and discussion

The results of the numerical simulation of TBVG inserts integrated heat exchanger tube are presented in Fig. 8.

The modified fluid flow structure due to the presence of TBVG insert with $PR = 1$, $PI = 25\%$, at $Re = 6000$, is shown in the form of 3D streamlines inside the tube in Fig. 8a. The presence of the TBVG insert causes a swirl flow inside the tube, resulting in better mixing of fluid flowing near the wall and in the tube's center. This new fluid flow pattern aids in the generation of high turbulence intensity, resulting in an improved rate of heat transfer. Furthermore, the presence of perforation causes jet impingement, which aids in the formation of a thinned thermal boundary layer and reduces flow hindrance to the fluid flow, lowering frictional losses. Because of the jet impingement through the perforations, the fluid velocity is also increased.

Figure 8b depicts the vortices created by the recirculation of fluid caused by TBVG inserts. The lambda 2 criterion is used to show the vortex core region and its direction. The vortex core in a tube is represented by the isosurface of a specific vortex strength. The vortices are produced downstream of each blade of the TBVG inserts resulting in three vortex core regions between two consecutive inserts, as shown in Fig. 8b. These vortices aid in the mixing up of fluid inside the tube and increase the fluid's residence time inside the tube.

Temperature contours with velocity vectors are shown at different transverse planes depicting the temperature transformation along the tube in Fig. 8c to demonstrate the temperature distribution through the tube due to the presence of TBVG inserts with $PR = 1$ and $PI = 25\%$ at $Re = 6000$. The presence of TBVG inserts increases the temperature of the air, and this increase in temperature is the result of a better mix-up of fluid flowing through the tube's center and wall regions.

Experimental results and discussion

The experimental results are plotted in graphical form, and the effects of each parameter on heat transfer and *f* are examined. Every insert with a different set of geometrical parameters for a specific flow rate performed differently and had a different impact on *Nu*, *f*, and TPF. In the following subsections, the effects of different geometrical and flow parameters on *Nu*, *f*, and TPF are discussed. The insert geometry and flow parameter values that are most desirable are determined by the heat exchanger's intended use.

Effect on the heat transfer

Figure 9a and b shows the effect of geometrical parameters such as *PR* and *PI* on *Nu* and enhancement in heat transfer over a smooth tube (Nu/Nu_s) with varying *Re*. With ascending *Re*, *Nu* shows an uptrend. This is because higher velocities of air in the tube produce more turbulence increasing heat transfer.

Since *PR* is proportional to the insert spacing, the number of TBVGs in the test section plays a significant role in generating turbulence in the fluid streams. As *PR* increases, heat transfer decreases significantly, and vice versa. This is primarily due to higher turbulence at lower *PR* values, which leads to a higher number of vortex and eddy generation in the fluid stream, ultimately resulting in a higher heat transfer value. Chamoli et al. [28], Nanan et al. [43], and Li et al. [44] reported similar results in their numerical investigations of inserts for various *PR* values. For $PR = 1$, the highest heat transfer is achieved. For $PI = 0\%$, a decrease in *Nu* is in the range of 10.7–12%, 12.2–14.8%, 19.2–20.5% for changes in PR from 1–2, 2–3, and 3–4, respectively.

It has been observed that as *PI* rises, the rate of heat transfer decreases slightly. Perforation in the insert causes jet impingement, which increases the heat transfer rate; however, perforation in the insert also reduces flow blockage, reducing the fluid's resident time, which decreases the heat transfer rate. These two aspects of perforation are of opposing nature. The aspect of flow blockage appears to dominate the jet impingement aspect of perforation in the current geometry. Convective heat transfer is observed to be maximum for 0% *PI*, which is due to the fact that the solid vortex generator has a large flow hindrance and generates strong vortex flow, which helps to generate a thinned thermal boundary layer over a tube wall and a high convective heat transfer rate. Skullong et al. [26] and Nakhchi et al. [30] reported similar results in their numerical investigation of the influence of perforation on *Nu*. When *PI* is increased from 0 to 25%, *Nu* decreases in the range of 4.6% to 9.7%. At $Re = 24{,}000$, the highest *Nu* of 252.5 is seen for $PI = 0\%$ and $PR = 1$. The range of heat transfer augmentation over smooth tube is 2.4–4.35 as shown in Fig. 9b.

Effect on the friction factor

The *f* value has a significant impact on such systems' thermal performance. Because thermal performance is inversely proportional to *f*, it is highly desirable to obtain the optimal configurations that result in the least amount of *f* penalty. Figure 9c and d shows the effects *of PR and PI on f* and f/f_s, respectively. Because *f* has an inverse relationship with the square of the fluid's velocity, the values of *f* show a downward trend as *Re* increases. The values of *f* decrease as *PR* increases and vice versa. This is due to the significant

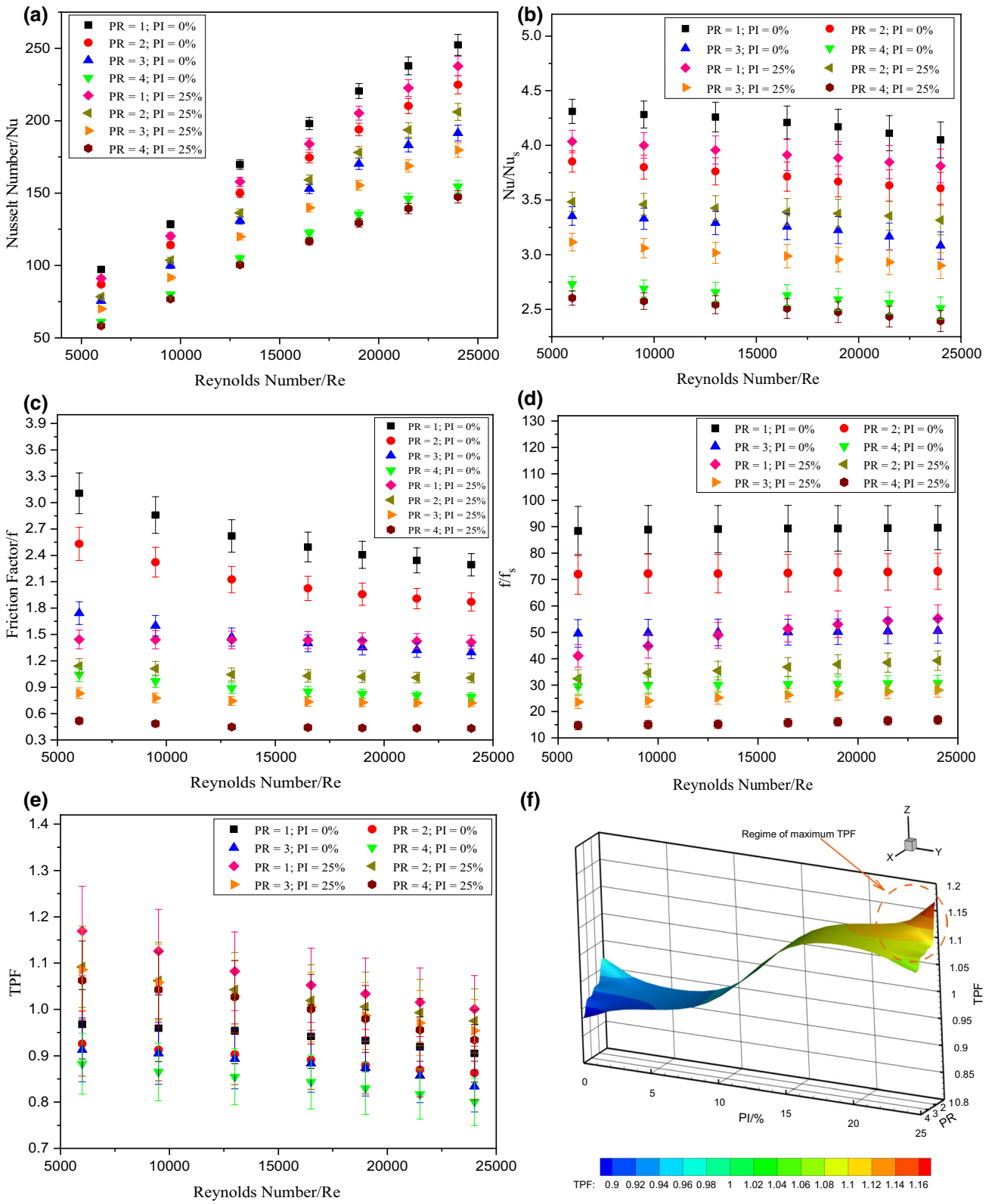

Fig. 9 Influence of different geometrical and flow parameters with error bars on: **a.** *Nu*, **b.** Nu/Nu_s, **c.** *f*, **d.** f/f_s, **e.** TPF. **f**. 3D surface plot of TPF at $Re = 6000$

Table 3 Statistical correlations for *Nu*, *f*, and TPF

Solid TBVG, $PI = 0\%$	Perforated TBVG, $PI = 25\%$
$\mathrm{Nu} = 0.2304(\mathrm{Re})^{0.695}(\mathrm{PR})^{-0.3177}$	$\mathrm{Nu} = 0.2165(\mathrm{Re})^{0.6976}(\mathrm{PR})^{-0.3034}$
$f = 24.0203(\mathrm{Re})^{-0.2198}(\mathrm{PR})^{-0.7336}$	$f = 3.9102(\mathrm{Re})^{-0.0982}(\mathrm{PR})^{-0.7429}$
$\mathrm{TPF} = 1.5085(\mathrm{Re})^{-0.0509}(\mathrm{PR})^{-0.0625}$	$\mathrm{TPF} = 3.1778(\mathrm{Re})^{-0.114}(\mathrm{PR})^{-0.0401}$

decrease in dynamical pressure head caused by low flow obstruction. For $PI = 0\%$, a decrease in f is in the range of 18.4%-18.8%, 30.7%-31.2%, 38.8%-40% for changes in PR from 1–2, 2–3, and 3–4, respectively.

The values of f decrease as PI increases, which is due to the fact that high perforation values impart very little flow blockage, resulting in a lower pressure drop. As PI increases from 0 to 25%, there is a significant decrease in f, with its values declining ranging from 38 to 54% for all parameters. At $Re = 6000$, the highest value of f, about 3.15, is found for the lowest PR of 1 and $PI = 0\%$; this results in a f enhancement of the order of about 88 times over a smooth tube. Furthermore, at $Re = 24{,}000$, where f/f_s is 15, the minimum value of f is 0.43 for $PR = 4$ and $PI = 25\%$.

Effect on the thermal performance factor

The improved heat transfer always accommodates the increased pumping power requirement, as shown by the above results for heat transfer and f. As a result, a new parameter called the thermal performance factor (TPF) is considered to accumulate both parameters at the same time. The TPF value for equal pumping power in a smooth tube is unity, and any value greater than unity indicated that the system is superior to a smooth tube. Figure 9e shows the TPF values for various values of Re, PR, and PI. The result shows that when the value of PR is reduced, the value of TPF increases. Heat transfer is high for lower PR values, resulting in a higher TPF.

The effect of PI on TPF is also quite distinct. The values of TPF show an upward trend as PI rises. This is due to a significant decrease in f as PI increases from 0 to 25%, with values ranging from 38 to 54%. TPF shows a downward trend as Re rises, which is due to a decrease in Nu/Nu_s as Re rises as opposed to f/f_s. The highest TPF value achieved is 1.16; this highest value was obtained for $PI = 25\%$, $PR = 1$, at $Re = 6000$.

TPF is in the range of (0.96–1.16), (0.92–1.09), (0.91–1.08), and (0.88–1.006) for values of PR of 1, 2, 3, and 4, respectively. In Fig. 9f, a 3D surface plot of the best parameters of the vortex generator insert shows that the maximum TPF of 1.16 is achieved at $PR = 1$ and $PI = 25\%$. This vortex generator is deemed to be the most efficient in terms of energy consumption.

Experimental correlations

Correlations for Nu, f, and TPF are developed based on the experimental results and include various experimentally tested parameters, as shown in Table 1. Table 3 shows the statistical correlations that have been developed. Figure 10 shows the deviations of predicted values from experimental values for Nu, f, and TPF, demonstrating that the developed correlations are in good agreement with experimental results, with maximum deviations of 8% for Nu, 15% for f, and 5% for TPF.

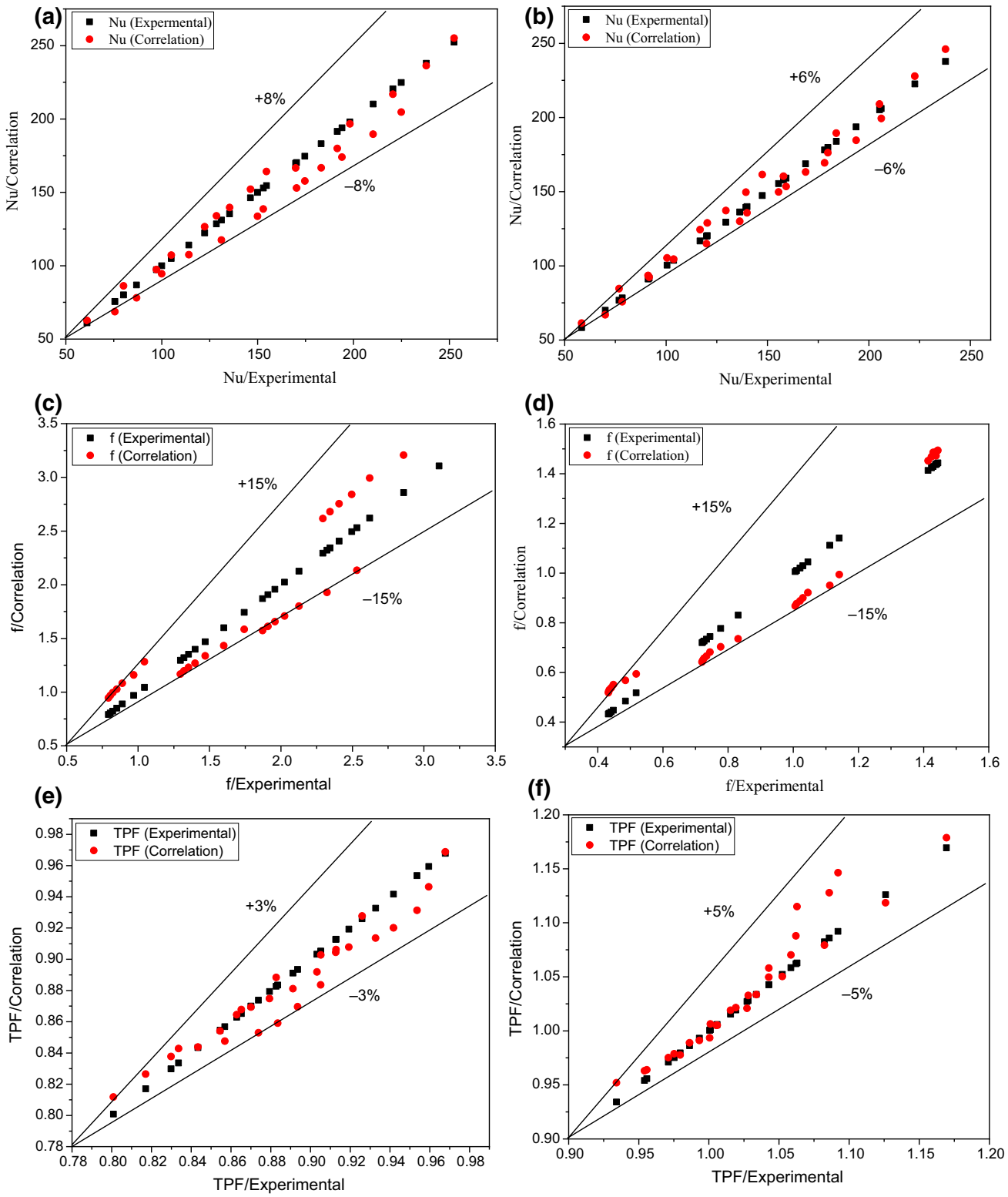

Fig. 10 Comparison of predicted values with experimental values for **a.** *Nu* for solid TBVG, **b.** *Nu* for perforated TBVG, **c**. *f* for solid TBVG, **d.** *f* for perforated TBVG, **e.** TPF for solid TBVG, **f**. TPF for perforated TBVG

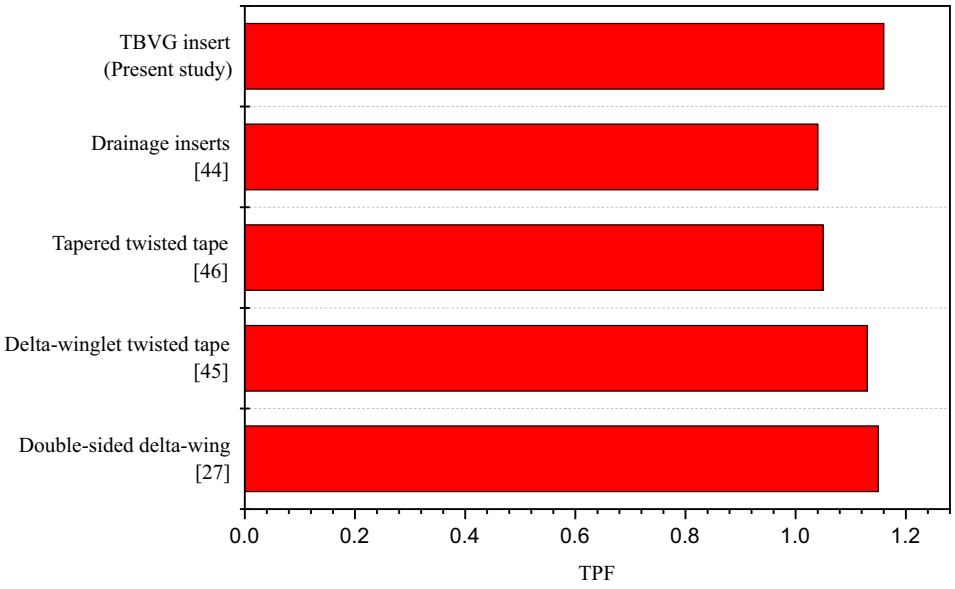

Fig. 11 Comparison of maximum TPF achieved for TBVG inserts with previous inserts

Comparison with previous inserts

The maximum TPF of present TBVG inserts is compared with some of the inserts investigated before by other researchers and is presented in Fig. 11. It could be seen from the plot that the maximum TPF of TBVG inserts is higher than the other inserts. The maximum TPF of TBVG insert is 0.87%, 11.54%, 2.65%, 10.48% higher than the maximum TPF of double-sided delta-wing tape (Wijayanta et al. [27]), drainage inserts (Li et al. [44]), delta-winglet twisted tape (Eiamsa-ard et al. [45]), tapered twisted tape (Piriyarungrod et al. [46]) respectively. Hence, one can infer that the TBVG inserts generally perform better than the other inserts that are compared.

Conclusions

A novel insert geometry is developed in this study to improve the thermal performance of a tube heat exchanger. The following conclusions are presented as a result of the current study.

- By generating recirculation and vortices in the fluid flow, TBVG inserts in a heat exchanger tube can achieve a better mix-up of fluid between core and at the wall region of fluid flow which helps in disrupting the thermal boundary layer at the wall region of a tube resulting in a better convective heat transfer.
- The convective heat transfer increases with an increase in *Re*. Values of *Nu* ascend as *PR* drops from 4 to 1. The maximum enhancement in *Nu* value for vortex generator embedded tube over smooth tube is about 4.35.
- Heat transfer decreases as *PI* increases due to a reduction in flow hindrance. For $Re = 6000$ and $PR = 2$, the highest reduction in heat transfer of 9.7% is observed as *PI* increases from 0 to 25%.
- *PI* and *PR* significantly affected the values of *f* due to their direct effect on flow blockages. With an increase in *Re*, there is a decrease in *f*, whereas, with a reduction in *PI* and *PR*, the trend is reversed. The highest enhancement in *f* of 88 times over smooth tube is achieved by using TBVG inserts.
- TBVG inserts with $PI = 25\%$ give better TPF values than at $PI = 0\%$ for all values of *PR*. A downtrend is seen in the values of TPF with an increase in the values of *Re*. The best TPF for TBVG inserts achieved is 1.16.
- Modifications of the inserts, such as changing the size of the TBVG insert or the angle of the blades of the insert, could be considered for further research that could lead to the improved thermal performance of the heat exchanger tube.

Appendix: Uncertainty analysis

Reynolds number

$$\mathrm{Re} = \frac{\rho \mathrm{VD}}{\mu}$$

$$\frac{\delta \mathrm{Re}}{\mathrm{Re}} = \left[\left(\frac{\delta \rho}{\rho} \right)^2 + \left(\frac{\delta V}{V} \right)^2 + \left(\frac{\delta D}{D} \right)^2 + \left(\frac{\delta \mu}{\mu} \right)^2 \right]^{0.5}$$

$$\frac{\delta \mathrm{Re}}{Re} = \left[\left(8.18 \times 10^{-4}\right)^2 + \left(7.43 \times 10^{-2}\right)^2 + \left(9.34 \times 10^{-4}\right)^2 + \left(5.042 \times 10^{-4}\right)^2\right]^{0.5}$$

$$\frac{\delta \mathrm{Re}}{\mathrm{Re}} = 0.0742$$

Hence, the uncertainty in Reynolds number is 7.42%.

Nusselt number

$$\mathrm{Nu} = \frac{h\mathrm{D}}{K}$$

$$\frac{\delta \mathrm{Nu}}{\mathrm{Nu}} = \left[\left(\frac{\delta h}{h}\right)^2 + \left(\frac{\delta D}{D}\right)^2 + \left(\frac{\delta K}{K}\right)^2\right]^{0.5}$$

$$\frac{\delta \mathrm{Nu}}{\mathrm{Nu}} = \left[(0.0283)^2 + (0.000941)^2 + (0.00527)^2\right]^{0.5}$$

$$\frac{\delta \mathrm{Nu}}{\mathrm{Nu}} = 0.0287$$

Hence, uncertainty in the Nusselt number is 2.87%.

Friction factor

$$f = \frac{2\left(\Delta_{\mathrm{p}}\right)_{\mathrm{d}} D}{4\rho L V^2}$$

$$\frac{\delta f}{f} = \left[\left(\frac{\delta V}{V}\right)^2 + \left(\frac{\delta \rho}{\rho}\right)^2 + \left(\frac{\delta D}{D}\right)^2 + \left(\frac{\delta L}{L}\right)^2 + \left(\frac{\delta\left(\Delta_{\mathrm{p}}\right)_{\mathrm{d}}}{\left(\Delta_{\mathrm{p}}\right)_{\mathrm{d}}}\right)^2\right]^{0.5}$$

$$\frac{\delta f}{f} = \left[(0.0742)^2 + (0.000821)^2 + (0.000939)^2 + (0.0000667)^2 + (0.00767)^2\right]^{0.5}$$

$$\frac{\delta f}{f} = 0.0744$$

Hence, uncertainty in the friction factor is 7.45%.

Authors contribution RB, KKSM, MK, and SC conceived and planned the experiments. RB carried out the experiments. RB and SC planned and carried out the numerical simulations. KKSM, MK, and SC contributed to the interpretation of the results. RB took the lead in writing the manuscript. All authors provided critical feedback and helped shape the research, analysis, and manuscript.

Funding Not applicable.

Declarations

Conflict of interest None.

References

1. El-Sayed SA, El-Sayed SA, Abdel-Hamid ME, Sadoun MM. Experimental study of turbulent flow inside a circular tube with longitudinal interrupted fins in the streamwise direction. Exp Thermal Fluid Sci. 1997;15(1):1–15. https://doi.org/10.1016/S0894-1777(96)00078-7.
2. Bas H, Ozceyhan V. Heat transfer enhancement in a tube with twisted tape inserts placed separately from the tube wall. Exp Thermal Fluid Sci. 2012;41:51–8. https://doi.org/10.1016/j.expthermflusci.2012.03.008.
3. Bhuiya MMK, Sayem ASM, Islam M, Chowdhury MSU, Shahabuddin M. Performance assessment in a heat exchanger tube fitted with double counter twisted tape inserts. Int Commun Heat Mass Transf. 2014;50:25–33. https://doi.org/10.1016/j.icheatmasstransfer.2013.11.005.
4. Bhuiya MMK, Chowdhury MSU, Shahabuddin M, Saha M, Memon LA. Thermal characteristics in a heat exchanger tube fitted with triple twisted tape inserts. Int Commun Heat Mass Transf. 2013;48:124–32. https://doi.org/10.1016/j.icheatmasstransfer.2013.08.024.
5. Promvonge P, Eiamsa-ard S. Heat transfer behaviors in a tube with combined conical-ring and twisted-tape insert. Int Commun Heat Mass Transf. 2007;34(7):849–59. https://doi.org/10.1016/j.icheatmasstransfer.2007.03.019.
6. Promvonge P. Thermal augmentation in circular tube with twisted tape and wire coil turbulators. Energy Convers Manage. 2008;49(11):2949–55. https://doi.org/10.1016/j.enconman.2008.06.022.
7. Eiamsa-Ard S, Kongkaitpaiboon V, Nanan K. Thermohydraulics of turbulent flow through heat exchanger tubes fitted with circular-rings and twisted tapes. Chin J Chem Eng. 2013;21(6):585–93. https://doi.org/10.1016/S1004-9541(13)60504-2.
8. Eiamsa-Ard S, Promvonge P. Thermal characteristics in round tube fitted with serrated twisted tape. Appl Therm Eng. 2010;30(13):1673–82. https://doi.org/10.1016/j.applthermaleng.2010.03.026.
9. Bhuiya MMK, Chowdhury MSU, Saha M, Islam MT. Heat transfer and friction factor characteristics in turbulent flow through a tube fitted with perforated twisted tape inserts. Int Commun Heat Mass Transf. 2013;46:49–57. https://doi.org/10.1016/j.icheatmasstransfer.2013.05.012.
10. Pal S, Saha SK. Laminar fluid flow and heat transfer through a circular tube having spiral ribs and twisted tapes. Exp Thermal Fluid Sci. 2015;60:173–81. https://doi.org/10.1016/j.expthermflusci.2014.09.005.
11. Zhang C, Wang D, Ren K, Han Y, Youjian Zhu Xu, Peng JD, Zhang X. A comparative review of self-rotating and stationary twisted tape inserts in heat exchanger. Renew Sustain Energy Rev. 2016;53:433–49. https://doi.org/10.1016/j.rser.2015.08.048.
12. Salem MR, Eltoukhey MB, Ali RK, Elshazly KM. Experimental investigation on the hydrothermal performance of a double-pipe heat exchanger using helical tape insert. Int J Therm Sci. 2018;124:496–507. https://doi.org/10.1016/j.ijthermalsci.2017.10.040.
13. Abolarin SM, Everts M, Meyer JP. The influence of peripheral U-cut twisted tapes and ring inserts on the heat transfer and pressure drop characteristics in the transitional flow regime. Int J Heat Mass Transf. 2019;132:970–84. https://doi.org/10.1016/j.ijheatmasstransfer.2018.12.051.
14. Chu W-X, Tsai C-A, Lee B-H, Cheng K-Y, Wang C-C. Experimental investigation on heat transfer enhancement with twisted tape having various V-cut configurations. Appl Therm Eng. 2020;172:115148. https://doi.org/10.1016/j.applthermaleng.2020.115148.

15. Fagr MH, Rishak QA, Mushatet KS. performance evaluation of the characteristics of flow and heat transfer in a tube equipped with twisted tapes of new configurations. Int J Therm Sci. 2020;153:106323. https://doi.org/10.1016/j.ijthermalsci.2020.106323.
16. Dagdevir T, Ozceyhan V. An experimental study on heat transfer enhancement and flow characteristics of a tube with plain, perforated and dimpled twisted tape inserts. Int J Thermal Sci. 2021;159:106564. https://doi.org/10.1016/j.ijthermalsci.2020.106564.
17. Chang SW, Wu PS, Liu JH. Aerothermal performance of square duct enhanced by twisted tape with inclined ribs and slots. Int J Heat Mass Transf. 2021;177:121547. https://doi.org/10.1016/j.ijheatmasstransfer.2021.121547.
18. Singh SK, Kumar A. Experimental study of heat transfer and friction factor in a double pipe heat exchanger using twisted tape with dimple inserts. Energy Sour Part A Recov Util Environ Effects. 2021. https://doi.org/10.1080/15567036.2021.1927248.
19. Promvonge P, Eiamsa-ard S. Heat transfer and turbulent flow friction in a circular tube fitted with conical-nozzle turbulators. Int Commun Heat Mass Transf. 2007;34(1):72–82. https://doi.org/10.1016/j.icheatmasstransfer.2006.08.003.
20. Kongkaitpaiboon V, Nanan K, Eiamsa-ard S. Experimental investigation of heat transfer and turbulent flow friction in a tube fitted with perforated conical-rings. Int Commun Heat Mass Transf. 2010;37(5):560–7. https://doi.org/10.1016/j.icheatmasstransfer.2009.12.015.
21. Gunes S, Ozceyhan V, Buyukalaca O. Heat transfer enhancement in a tube with equilateral triangle cross sectioned coiled wire inserts. Exp Thermal Fluid Sci. 2010;34(6):684–91. https://doi.org/10.1016/j.expthermflusci.2009.12.010.
22. Kongkaitpaiboon V, Nanan K, Eiamsa-ard S. Experimental investigation of convective heat transfer and pressure loss in a round tube fitted with circular-ring turbulators. Int Commun Heat Mass Transf. 2010;37(5):568–74. https://doi.org/10.1016/j.icheatmasstransfer.2009.12.016.
23. Eiamsa-ard S, Promvonge P. Influence of double-sided delta-wing tape insert with alternate-axes on flow and heat transfer characteristics in a heat exchanger tube. Chin J Chem Eng. 2011;19(3):410–23. https://doi.org/10.1016/S1004-9541(11)60001-3.
24. Kumar A, Singh S, Chamoli S, Kumar M. Experimental investigation on thermo-hydraulic performance of heat exchanger tube with solid and perforated circular disk along with twisted tape insert. Heat Transf Eng. 2018;40(8):616–26. https://doi.org/10.1080/01457632.2018.1436618.
25. Singh SK, Kumar M, Kumar A, Gautam A, Chamoli S. Thermal and friction characteristics of a circular tube fitted with perforated hollow circular cylinder inserts. Appl Therm Eng. 2018;130:230–41. https://doi.org/10.1016/j.applthermaleng.2017.10.090.
26. Skullong S, Promvonge P, Thianpong C, Jayranaiwachira N, Pimsarn M. Thermal performance of heat exchanger tube inserted with curved-winglet tapes. Appl Therm Eng. 2018;129:1197–211. https://doi.org/10.1016/j.applthermaleng.2017.10.110.
27. Wijayanta AT, Yaningsih I, Aziz M, Miyazaki T, Koyama S. Double-sided delta-wing tape inserts to enhance convective heat transfer and fluid flow characteristics of a double-pipe heat exchanger. Appl Therm Eng. 2018;145:27–37. https://doi.org/10.1016/j.applthermaleng.2018.09.009.
28. Chamoli S, Ruixin Lu, Xie J, Peng Yu. Numerical study on flow structure and heat transfer in a circular tube integrated with novel anchor shaped inserts. Appl Therm Eng. 2018;135:304–24. https://doi.org/10.1016/j.applthermaleng.2018.02.052.
29. Gururatana S, Skullong S. Experimental investigation of heat transfer in a tube heat exchanger with airfoil-shaped insert. Case Studies Thermal Eng. 2019;14:100462. https://doi.org/10.1016/j.csite.2019.100462.
30. Nakhchi ME, Esfahani JA, Kim KC. Numerical study of turbulent flow inside heat exchangers using perforated louvered strip inserts. Int J Heat Mass Transf. 2020. https://doi.org/10.1016/j.ijheatmasstransfer.2019.119143.
31. Liang Y, Liu P, Zheng N, Shan F, Liu Z, Liu W. Numerical investigation of heat transfer and flow characteristics of laminar flow in a tube with center-tapered wavy-tape insert. Appl Thermal Eng. 2019;148:557–67. https://doi.org/10.1016/j.applthermaleng.2018.11.090.
32. Hong Y, Juan Du, Wang S, Ye W-B, Huang S-M. Turbulent thermal-hydraulic and thermodynamic characteristics in a traverse corrugated tube fitted with twin and triple wire coils. Int J Heat Mass Transf. 2019;130:483–95. https://doi.org/10.1016/j.ijheatmasstransfer.2018.10.087.
33. Paneliya S, Khanna S, Mankad V, Ray A, Prajapati P, Mukhopadhyay I. Comparative study of heat transfer characteristics of a tube equipped with x-shaped and twisted tape insert. Mater Today Proc. 2020;28:1175–80. https://doi.org/10.1016/j.matpr.2020.01.103.
34. Bahuguna R, Mer KKS, Kumar M, Chamoli S. Thermohydraulic performance and second law analysis of a tube embedded with multiple helical tape inserts. Energy Sour Part A Recov Util Environ Effects. 2021. https://doi.org/10.1080/15567036.2021.1904057.
35. Singh BP, Bisht VS, Bhandari P. Numerical study of heat exchanger having protrusion and dimple roughened conical ring inserts. In: Sikarwar BS, Sundén B, Wang Q, editors. Advances in fluid and thermal engineering. Singapore: Springer; 2021. p. 151–61.
36. Zarei R, Razzaghi K, Shahraki F. Experimental characterization of heat transfer enhancement in a circular tube fitted with Koflo Blade™ inline mixer. Chem Eng Process Process Intensif. 2021;166:108508. https://doi.org/10.1016/j.cep.2021.108508.
37. Ebrahimi A, Naranjani B. An investigation on thermo-hydraulic performance of a flat-plate channel with pyramidal protrusions. Appl Thermal Eng. 2016;106:316–24. https://doi.org/10.1016/j.applthermaleng.2016.06.015.
38. Ebrahimi A, Roohi E. Numerical study of flow patterns and heat transfer in mini twisted oval tubes. Int J Mod Phys C. 2015;26(12):1550140. https://doi.org/10.1142/S0129183115501405.
39. Manoram RB, Sathiya Moorthy R, Ragunathan R. Investigation on influence of dimpled surfaces on heat transfer enhancement and friction factor in solar water heater. J Therm Anal Calorim. 2021;145(2):541–58. https://doi.org/10.1007/s10973-020-09746-0.
40. Bhattacharyya S, Benim AC, Bennacer R, Dey K. Influence of broken twisted tape on heat transfer performance in novel axial corrugated tubes: experimental and numerical study. Heat Transfer Eng. 2022;43(3–5):437–62. https://doi.org/10.1080/01457632.2021.1875168.
41. Kline SJ, McClintock FA. Describing uncertainties in single sample experiments. Mech Eng. 1953;75:385–7.
42. Versteeg HK, Malalasekera W. An introduction to computational fluid dynamics: the finite volume method. Harlow: Pearson/Prentice Hall; 2008.
43. Nanan K, Thianpong C, Pimsarn M, Chuwattanakul V, Eiamsa-ard S. Flow and thermal mechanisms in a heat exchanger tube inserted with twisted cross-baffle turbulators. Appl Therm Eng.

2017;114:130–47. https://doi.org/10.1016/j.applthermaleng.2016.11.153.
44. Li P, Liu P, Liu Z, Liu W. Experimental and numerical study on the heat transfer and flow performance for the circular tube fitted with drainage inserts. Int J Heat Mass Transf. 2017;107:686–96. https://doi.org/10.1016/j.ijheatmasstransfer.2016.11.094.
45. Eiamsa-ard S, Wongcharee K, Eiamsa-ard P, Thianpong C. Heat Transfer enhancement in a tube using delta-winglet twisted tape inserts. Appl Therm Eng. 2010;30(4):310–8. https://doi.org/10.1016/j.applthermaleng.2009.09.006.
46. Piriyarungrod N, Eiamsa-ard S, Thianpong C, Pimsarn M, Nanan K. Heat transfer enhancement by tapered twisted tape inserts. Chem Eng Process. 2015;96:62–71. https://doi.org/10.1016/j.cep.2015.08.002.